Received: 13 July 2020 | Revised: 29 October 2020 | Accepted: 2 November 2020

DOI: 10.1002/elsa.202000010

ELECTROCHEMICAL SCIENCE ADVANCES Open Access | WILEY-VCH

FULL ARTICLE

Coral-like nitrogen doped carbon derived from polyaniline-silicon nitride hybrid for highly active oxygen reduction electrocatalysis

Ana Maria Borges Honorato[1,2] | **Mohd. Khalid**[3] | **Luiz Antonio Pessan**[2,4]

[1] Center of Advanced Science and Engineering for Carbon (Case4Carbon), Department of Macromolecular Science and Engineering, Case Western Reserve University, Cleveland, Ohio, USA

[2] Graduate Program in Materials Science and Engineering, Federal University of São Carlos, São Carlos, Sao Paulo, Brazil

[3] Institute of Chemistry of São Carlos, University of São Paulo, São Carlos, Sao Paulo, Brazil

[4] Department of Materials Engineering, Federal University of São Carlos, São Carlos, Sao Paulo, Brazil

Correspondence
Ana Maria Borges Honorato, Center of Advanced Science and Engineering for Carbon (Case4Carbon), Department of Macromolecular Science and Engineering, Case Western Reserve University, 10900 Euclid Avenue, Cleveland, OH 44106, USA.
Email: aborgeshonorato@gmail.com; mkansarister@gmail.com; pessan@ufscar.br

Funding information
Fundação de Amparo à Pesquisa do Estado de São Paulo, Grant/Award Number: 2017/0433-5; Coordenação de Aperfeiçoamento de Pessoal de Nível Superior, Grant/Award Number: 001

Abstract

In this work, a coral-like nitrogen-doped carbon electrocatalyst has been prepared via self-assembly oxidative polymerization of aniline monomers onto silicon nitride (Si_3N_4) nanospheres, followed by carbonization. The prepared catalyst at 900°C (denoted as NC-900) shows excellent oxygen reduction reaction (ORR) activity by achieving an onset potential (η) of 0.90 V versus reversible hydrogen electrode (RHE) and half wave potential ($E_{1/2}$) of 0.82 V versus RHE comparable to that of the commercial Pt/C (η = 0.99 V vs. RHE and $E_{1/2}$ = 0.87 V vs RHE) and even outperforming many carbon-based electrocatalysts recently reported in the literature. The catalyst NC-900 also displays better stability and resistance toward methanol crossover effect than Pt/C in alkaline solution. The high ORR performance of NC-900 catalyst was associated with high content of nitrogen species and hierarchical mesoporous structure that facilitate high electron and mass transport.

KEYWORDS
electrocatalysis, nitrogen-doped carbon, coral-like structure, ORR

1 | INTRODUCTION

Over the past decades, enormous efforts have been devoted on developing renewable clean energy conversion and storage systems, such as fuel cells and metal-air batteries.[1–3] One of key processes of these energy systems is the oxygen reduction reaction (ORR), which is a multistep sluggish kinetic reaction, that occurs at cathode via adsorbing oxygen intermediates on the active sites of electrocatalyst.[4,5] Therefore, the ORR of an electrocatalyst greatly depends on the interaction strength between the active sites and reaction intermediates. So far, the leading electrocatalysts

for ORR have been recognized as platinum (Pt) based, which show highest positive onset potential and half wave potential. Unfortunately, Pt-based catalysts face several challenges related to unaffordable cost, susceptibility to poisoning, and shortage in nature, which impede their widespread commercial utilization.[6,7] On the other hand, the nonprecious metals and their alloys/oxides have been extensively studied but they are also not free from many disadvantages such as low stability in harsh electrolyte environment, poor selectivity, and succeptiblity toward gas poisoning.[8–10] To mitigate these issues, it is highly desirable to develop alternative electrocatalysts with low cost, high perfomance, and stability.

In this context, doped carbonaceous materials have emerged as promissing alternatives to precious and nonprecious metal-based ORR electrocatalysts.[11–13] Doping of carbon materials, especially with N heteroatom, induces high positive charge density on coordinated neighboring carbon atoms due to the large difference in electronegativity and thus facilitates the adsorption of oxygen on catalyst surface.[14] It has also been reported that the charge redistribution induced by nitrogen doping leads to different configuration with adjacent carbon atoms forming pyridinic-N, pyrrolic-N, quarternary-N, and oxidized-N species, and each have different contribution in electrocatalytic reaction.[13,14] Co-doping of heteroatoms in carbon network has also been reported for better catalytic activity than the single heteroatom-doped carbon counterpart due to the synergistic effect of two different heteroatoms. For an ideal carbon-based electrocatalyst, not only doping but other features are also important, such as high conductivity and porosity to create fast mass transport channels.

In our latest work,[15] we have shown a highly entangled fibrous-like N and S co-doped carbon electrocatalyst obtained from the combination of polyaniline and polythiophene precursors followed by carbonization, which demonstrated outstanding ORR performance revealing the onset potential of 0.94 V versus reversible hydrogen electrode (RHE) very close to the benchmark Pt/C (1 V vs. RHE). In another study, Huang and co-workers[16] synthesized carbon nanocages using the precursors of polyethylene oxide-polypropylene oxide-polyethylene oxide (PEO-PPO-PEO) three-block copolymer (F127) and $Zn(OH)_2$ for ORR catalysis in alkaline solution. Taking the advantages of high surface area (1011 $m^2\ g^{-1}$), optimized pyrolysis condition, and unique morphological structure, the obtained carbon nanocages exhibited excellent onset potential and half wave potential of 0.89 and 0.71 V versus RHE, respectively. The nitrogen-doped carbon nanoflowers were also synthesized using the precursors of pyrrole, aniline, and phenanthroline.[17] The optimal catalyst derived from phenanthroline at 900°C (N-CNF-PHEN-900) comprising large specific surface area (1039 $m^2\ g^{-1}$) showed superior ORR activity by surpassing the benchmark Pt/C catalyst with 30 mV half wave potential in alkaline solution. According to the above considerations, building hierarchical porous carbon electrocatalyst have shown benefit in electron transfer and mass diffusion for enhancing catalytic performance of the electrocatalysts.

Herein, we synthesized a hierarchical coral-like nitrogen-doped carbon using self-assembly oxidative polymerization of aniline monomers onto silicon nitride, followed by a simple one-step carbonization process. The as-synthesized hierarchical coral-like nitrogen-doped carbon displayed excellent catalytic activity, stability, and tolerance toward methanol poisoning effect in alkaline solution. The high catalytic activity of as-prepared catalyst was associated with high content of nitrogen species and mesoporous structure, which promote rapid mass/electron transport. This work offers an effective strategy to develop promising electrocatalyst for ORR using polyaniline and silicon nitride precursors.

2 | EXPERIMENTAL SECTION

2.1 | Chemicals

Aniline monomer (99.5%), silicon nitride (Si_3N_4 nanosphere) with average size of ~20 nm, ammonium persulfate ($(NH_4)_2\ S_2O_8$), potassium hydroxide (KOH, 99%), and Nafion solution (5 wt% in ethanol) were purchased from Sigma-Aldrich. The Pt/C (20 wt%) was from E-TEK. The water was purified by the equipment of Milli-Q Advantage A10, Merck Millipore, with a resistivity of 18.25 MΩ cm^{-1}.

2.2 | Synthesis of coral-like nitrogen-doped carbon

First, aniline monomers were polymerized onto the surface of Si_3N_4 nanospheres as follows: 0.2 g of Si_3N_4 nanospheres were dispersed in 30 mL of deionized water and sonicated for 2 h at room temperature. An anilinium solution was prepared in a separate beaker by adding 2.2 mmol of aniline monomers into 8.2 mmol of HCl solution under continuous stirring using Teflon coated magnetic bar, following the procedure of earlier reported work.[18] The well-mixed anilinium solution was then poured into the dispersion of Si_3N_4 nanospheres at 0°C under vigorous stirring for 2 h. Afterward, the mixture of Si_3N_4-anilinium was injected into 50 mL of chloroform under constant stirring and kept the beaker in dry ice bath inside the frigorific room at −10°C. The precooled solution (50 mL)

of the oxidizing agent (ammonium persulfate, 0.88 M) was slowly added into the mixture of Si_3N_4-anilinium and left for polymerization inside the frigorific room at −10°C for 14 h. After polymerization, a green color product was obtained, which was thoroughly washed with deionized water and centrifuged for five times. Then the product was collected in plastic tubes and freeze dried for 3 days. The resulting hybrid material constituted with polyaniline and Si_3N_4 nanospheres was carbonized. The carbonization of the material was processed for two different temperatures 900°C and 1000°C under argon atmosphere with ramp rate of 2°C/min for 3 h. After carbonization, the material turned into a black-colored powder. The final samples were named as NC-900 and NC-1000, according to the temperatures of carbonization.

2.3 | Physical characterization

The surface morphology of the samples was characterized by transmission electron microscopy (TEM) using JEM2100 LaB_6 200 kV. The corresponding EDX had the sensitivity of 0.1 wt%, which cannot rule out the presence of any possible metal impurities at a lower level than the detection limit of EDX measurements. The structural features of the samples were investigated by several techniques, such as X-ray diffraction (XRD, Bruker, D8 Advance) with Cu Kα radiation source ($\lambda = 1.54$ Å), Raman measurement (Renishaw) with wavelength of 633 nm as an excitation source, X-ray photoelectron spectroscopy (XPS, PHI-5300 ESCA spectrometer, Perkin Elmer) with 300W Al Kα radiation, and Brunauer–Emmett–Teller (BET; TriStar II 3020, version 2) for surface area.

2.4 | Electrochemical characterization

The electrocatalytic activities of the samples were tested in N_2- and O_2-saturated 0.1 M KOH solution employing standard three-electrode cell setup using electrochemical workstation of CHI-60E at room temperature. The reference electrode of Hg/Hg_2Cl_2, (KCl saturated) and counter electrode of graphite rod (Alfa Aesar, 99.999%) were used. The catalyst ink was prepared by dispersing 2 mg of catalyst into 400 µL of ethanol and 40 µL of 5 wt% Nafion solution and ultrasonicated for 30 min to obtain a homogeneous mixture at room temperature. To prepare the working electrode, 20 µL of ink was drop-casted onto precleaned glassy carbon electrode (area 0.196 cm^2), which gives loading of catalyst ~0.075 mg. The measured potentials versus Hg/Hg_2Cl_2 were converted to the RHE via Nernst equation ($E_{vs\ RHE} = E_{vs\ Hg/Hg2Cl2} + 0.095 + 0.059$ pH). Koutecký–Levich (K–L) plots were obtained by linear fitting of the reciprocal rotating speed versus reciprocal current density, collected at different potentials. The average electron transfer number (n) per oxygen molecule involved in a typical ORR process was calculated from the slope of K–L plots using the following equation[14]:

$$\frac{1}{j} = \frac{1}{j_k} + \frac{1}{B\omega^{\frac{1}{2}}}, \tag{1}$$

where j is the measured current density, j_k is the kinetic current density, ω is the electrode rotating rate in rpm, and B is the reciprocal of the slope obtained from the K–L plots based on the following equation:

$$B = 0.2nFAv^{-\frac{1}{6}}C_{O2}(D_{O2})^{\frac{2}{3}}, \tag{2}$$

where n is the number of transferred electron per oxygen molecule, F is the Faraday constant (96,485 C mol^{-1}), D_{O2} is the diffusion coefficient of O_2 in 0.1 M KOH (1.9×10^{-5} cm^2 s^{-1}), v is the kinetic viscosity of the electrolyte (0.01 cm^2 s^{-1}), and C_{O2} is the concentration of O_2 (1.2×10^{-6} mol cm^{-3}). The constant 0.2 is adopted when the rotating speed is in rpm.

The hydrogen peroxide yield (% H_2O_2) and corresponding electron transfer number (n) were calculated by the following equations:

$$\%H_2O_2 = 200 \times \frac{I_r}{(NI_d + I_r)}, \tag{3}$$

$$n = \frac{4NI_d}{(NI_d + I_r)}. \tag{4}$$

where I_d and I_r are the disc and ring current, and N is the current collection efficiency of the ring electrode, which was determined to be 0.37.

3 | RESULTS AND DISCUSSION

A schematic representation for the synthesis of catalyst is shown in **Figure 1**. The anilinium ions electrostatically interacted all around the nanospheres of Si_3N_4 and formed a self-assembly of anilinium ions and Si_3N_4 nanospheres in the aqueous/chloroform interface.[18,19] Upon addition of oxidizing agent ($(NH_4)_2$ S_2O_8), the anilinium ions start polymerizing on Si_3N_4 nanospheres; as the polymer chains grow, they come in contact with the interface of aqueous and organic-chloroform phases, where the segments of amine (hydrophilic) phenyl (hydrophobic) avoid the solubility in both aqueous and organic phases and as a result polymer chains act as an interfacial stabilizer.[19] According to Kim et al. [18] an aqueous/

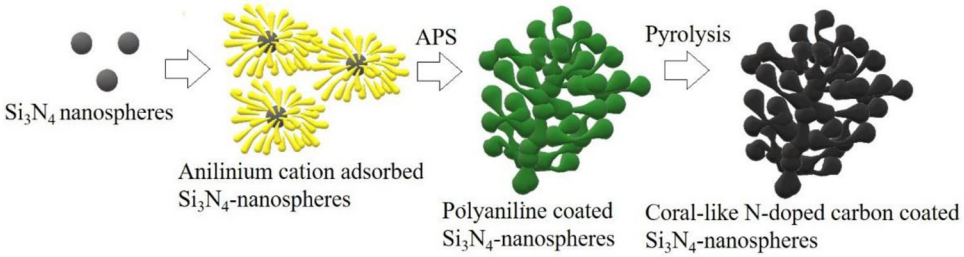

FIGURE 1 Synthetic protocol for the preparation of coral-like nitrogen-doped carbon coated on Si_3N_4nanospheres

organic interface system provides para-direction polymerized structure, which results in a highly conductive polyaniline.

Figure 2a-d shows the TEM images of sample NC-900 at different magnifications, which clearly displayed a coral-like structure comprising the coral type branches of several nanometers in length. The Si_3N_4 nanosphere can also be observed with average size of ~16 nm (**Figure 2d**). Sample NC-1000 also showed coral-like morphological structure of the catalyst, as shown in Figure S1. Such unique morphological design of catalyst can increase the specific surface area of the catalyst. The energy dispersive X-ray spectroscopy (EDX) was investigated for elemental mappings of C, Si, N, and O, which showed homogeneous distribution and composition of all elements (**Figure 2e** and Figure S2) that could be beneficial for promoting high catalytic activity of the electrocatalyst.

Further, the structural characterizations of the materials were investigated by XRD, Raman spectroscopy, nitrogen-adsorption/desorption isotherm, and XPS. The XRD patterns of NC-900 and NC-1000 (**Figure 3a**) represent the most relevant peaks at $2\theta = 24^{o}$ and 43^{o}, indicating that the both samples consist of graphitized carbon, which can greatly improve the electronic conductivity of the materials.[20] Raman spectra of NC-900 and NC-1000 (**Figure 3b**) show D- and G-bands at 1330 and 1592 cm^{-1}, respectively.[21] The calculated peak intensities (I_D/I_G) were 0.894 (NC-900) and 0.886 (NC-1000), further suggesting that there is a considerable graphitized carbon in the samples. BET surface area and pore size distribution were investigated by a nitrogen adsorption/desorption analysis. As shown in **Figure 3c**, both samples show the type IV adsorption isotherm, manifesting high mesoporous structure of the materials.[22] BET specific surface area was measured to be 403 and 420 $m^2\ g^{-1}$ for NC-900 and NC-1000, respectively. Sample NC-1000 showed slightly higher specific surface area than the NC-900, which could be due to the higher carbonization temperature of 1000°C. Dollimore Heal pore distribution plot was derived from the nitrogen desorption isotherm (**Figure 3d**), and also showed that the majority of mesopores with diameter were in the range of 10–50 nm in the samples.

XPS survey spectra of NC-900 and NC-1000 showed the presence of C, Si, O, and N elements in **Figure 4a**. The nitrogen element comes from the source of polyaniline and silicon nitride precursors. The nitrogen contents for NC-900 and NC-1000 were found to be 18% and 16%, respectively. Note that the nitrogen content was found slightly less in sample NC-1000, this is because the higher temperature can cause the loss of some nitrogen content from the sample. Deconvolution of N1s XPS spectra (**Figure 4b**) of NC-900 showed 70.4% pyridinic-N (398 eV), 29% pyrrolic-N (399 eV), and 0.6% quaternary-N (400 eV). Although the deconvolution of N1s XPS spectra for NC-1000 (**Figure 4c**) showed 79.5% pyridinic-N (397 eV) and 20.5% pyrrolic-N species but without quaternary-N. It has been shown in previous studies that the pyridinic-N was responsible for high catalytic onset potential for ORR via four-electron path.[23,24] As pyridinic-N species contributes a single electron pair in the plane of carbon lattice by weakening the O-O bond for oxygen reduction.[25] Besides that, in order to correlate the content of nitrogen species with the catalytic performance, one must take into consideration that the co-existence of pyridinic-N and quaternary-N in NC-900 can also generate synergistic effect due to their different electronic configurations, which could greatly improve the catalytic performance of the catalyst material.[26–31]

The electrochemical experiments for the samples were conducted using three-electrode cell configuration to evaluate ORR performance. Pristine Si_3N_4 nanospheres and commercial Pt/C (20 wt%) were also evaluated for comparison purpose. To investigate the electrocatalytic activities of the samples, cyclic voltammogram (CV) was carried out in N_2- and O_2-saturated 0.1 M KOH solution with a scan rate of 10 mV s^{-1}. As shown in **Figure 5a** and Figure S3a, the peak current for the oxygen reduction was gained in O_2-saturated 0.1 M KOH solution. The insignificant background current in N_2-saturated 0.1 M KOH solution verifies that the observed reduction current peak in O_2-saturated 0.1 M KOH solution was due to the reduction of dissolved oxygen in electrolyte. As shown in **Figure 5b**, the linear sweep voltammetry (LSV) at rotating speed of 1200 rpm, the NC-900 exhibits onset potential (η) of 0.90 V versus RHE and half wave potential ($E_{1/2}$) of

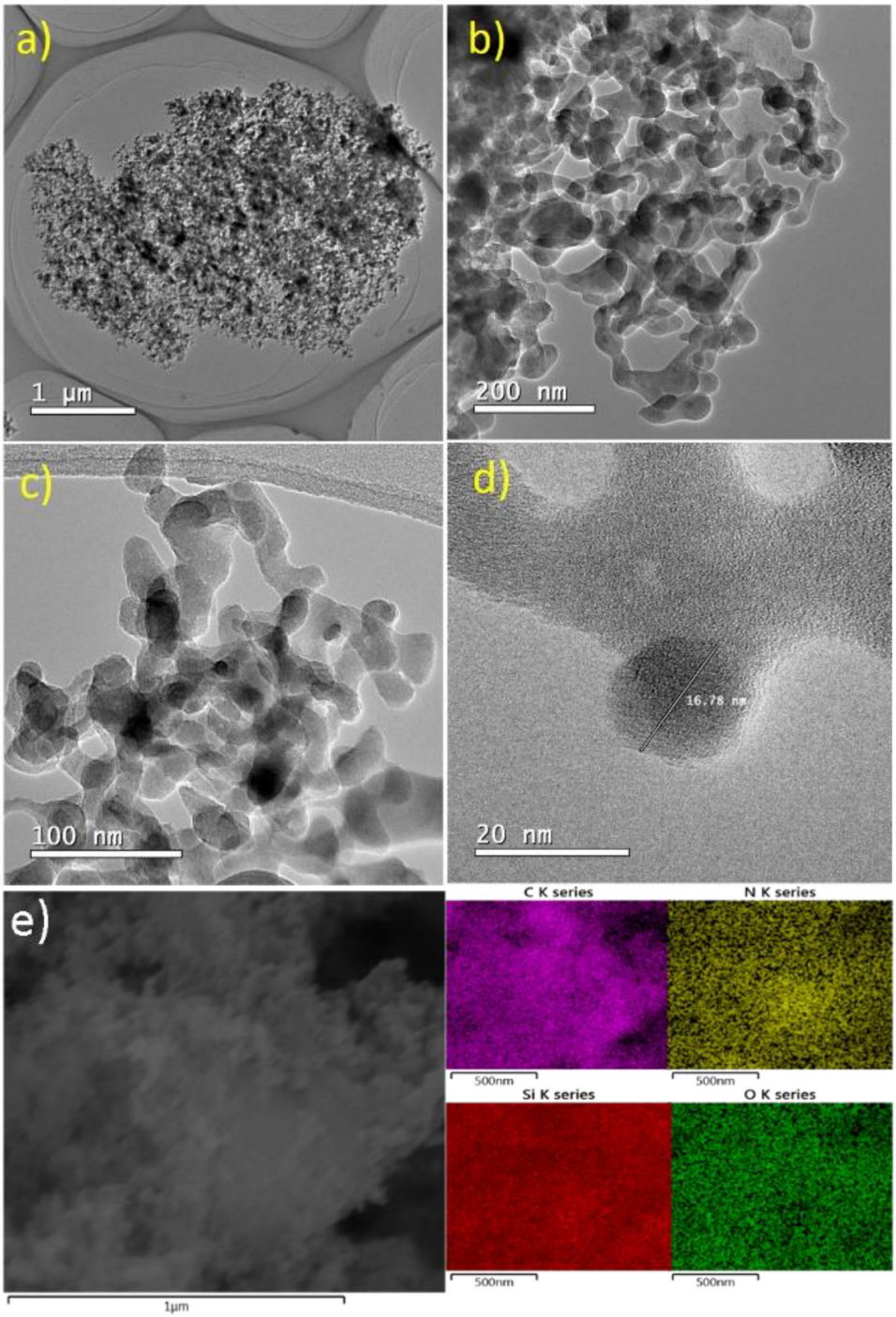

FIGURE 2 Morphological analysis. (a–d) TEM images of the sample NC-900 at different magnifications, and (e) corresponding EDX mapping images of C, Si, N, and O elements

0.82 V versus RHE, which was more positive than that of the counterpart NC-1000 (η = 0.88 V vs. RHE and $E_{1/2}$ = 0.80 V vs. RHE). The obtained onset potential (η = 0.90 V vs. RHE) for NC-900 is appreciable in comparison with benchmark Pt/C (η = 0.99 V vs. RHE and $E_{1/2}$ = 0.87 V vs. RHE) and even superior to that of many reported ORR electrocatalysts based on carbon nanomaterials, as presented in Table S1. Meantime, the negligible performance of the pristine Si_3N_4 nanospheres indicates that the catalytic ORR performances of the samples NC-900 and NC-1000 are originating merely from the nitrogen-doped carbon. The better ORR performance of NC-900 as compared to NC-1000 was associated with the high content of pyridinic-N, as revealed by XPS analysis (**Figure 4b**), which improves the onset potential of catalyst.[24] Notably, the additional quaternary-N species in NC-900

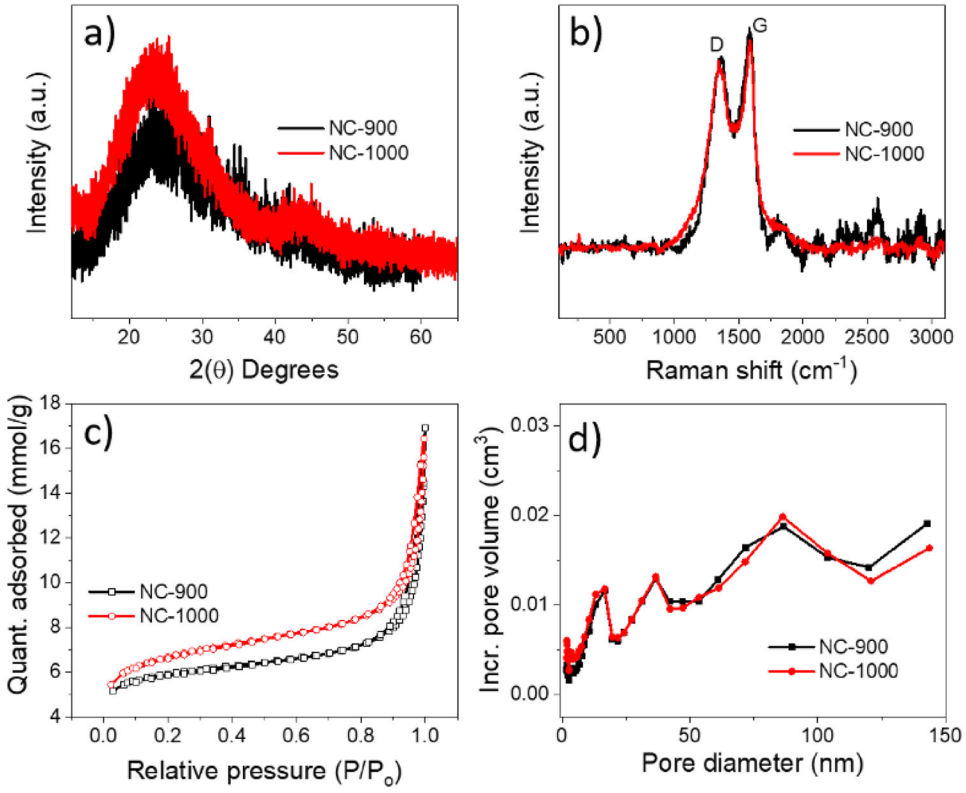

FIGURE 3 Physical characterizations. (a) XRD patterns of NC-900 and NC-1000, (b) Raman spectra of NC-900 and NC-1000, (c) nitrogen adsorption-desorption isotherm of NC-900 and NC-1000, and (d) corresponding pore size distribution curves for NC-900 and NC-1000

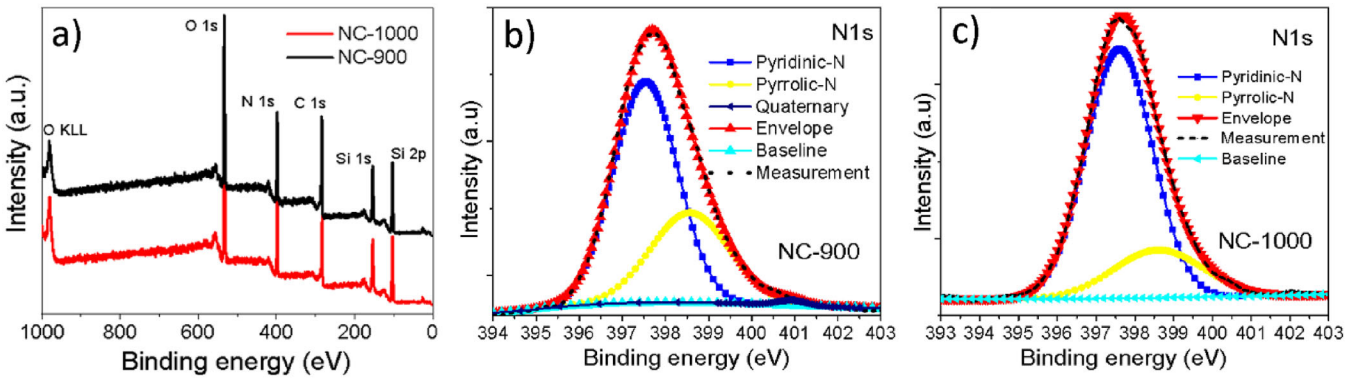

FIGURE 4 (a) XPS survey spectra of NC-900 and NC-1000, (b) HR-XPS spectra of N 1s of NC-900, and (c) HR-XPS spectra of N 1s of NC-1000

may increase the limiting current density, while pyrrolic-N has little impact on electrocatalytic performance of carbon materials.[31] These results are consistent with previously reported works, where pyridinic-N and its synergistic contribution with other nitrogen species have been proven for high ORR activity.[25–27] Further, the LSV test was investigated using various rotating speeds, ranging from 400 to 2400 rpm at scan rate of 10 mV s^{-1} (**Figure 5c** and Figure S3b). The cathodic current increases with increasing rotational speed with high diffusion current density for NC-900 compared to the NC-1000, suggesting a good diffusion-controlled oxygen reduction and first-order kinetic of NC-900 for ORR in alkaline solution.[24,32,33] **Figure 5d** shows the corresponding K–L plot (j^{-1} vs. $\omega^{-1/2}$) of NC-900 and Figure S3c for NC-1000, derived from the LSV curves between the potential range of 0.2–0.6 V versus RHE at different rotating speeds to get mass-transport ORR kinetics using Equation (1). The K–L plot shows the parallel fitting correlation, further suggesting the first-order reaction kinetic against the concentration of

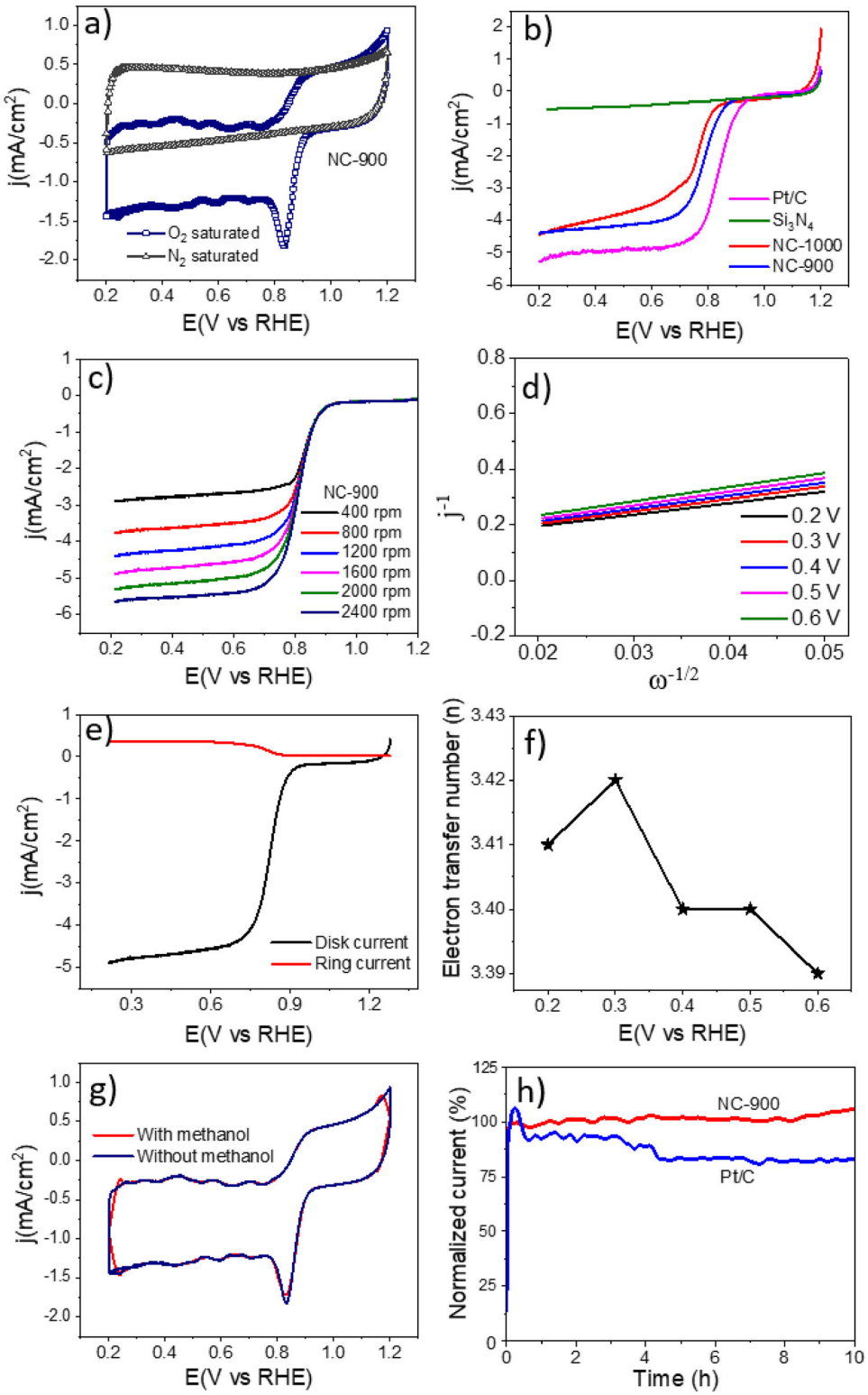

FIGURE 5 Electrochemical analysis. (a) CV curves of NC-900 in N_2-/O_2-saturated 0.1 M KOH solution; (b) LSV curves of NC-900, NC-1000, Pt/C, and pristine Si_3N_4nanospheres; (c) LSV curves of NC-900 at different rotating speeds, (d) Koutecký–Levich plot derived from LSV curves of NC-900, (e) ring and disc currents on RRDE for NC-900 at 1600 rpm, (f) corresponding electron transfer number from RRDE, (g) CV curves with and without CH_3OH for NC-900, and (h) current–time (*i*–*t*) chronoamperometric curves for NC-900 and Pt/C catalysts

dissolved oxygen and potential-dependent electron transfer rate.[34,35] According to K–L plot, the highest electron transfer number (calculated from Equation (2)) for NC-900 was measured to be 3.50, revealing a mixed 2- and 4-electron transfer path, as represented in Figure S4 at different potential values for NC-900, while NC-1000 showed an average electron transfer number value of 2.73 (Figure S3d). Further, ORR activity of the samples was investigated from the generated peroxide species on rotating ring disc electrode (RRDE) at 1600 rpm (**Figure 5e** and Figure S5a), where the obtained ring current was much lower than the disc current, signifying the high limited current density for ORR. The sample NC-900 generated lower amount of peroxide species and the higher electron transfer number compared to that of sample NC-1000. As shown in the Figure S6, the yield of peroxide for NC-900 was calculated near to 15%, while NC-1000 showed more than 23% (Figure S5b), indicating that the NC-900 is more selective toward ORR. According to the disc and ring currents (Equations (3) and (4)), the highest electron transfer numbers were measured to be 3.42 and 3.03 for NC-900 and NC-1000, respectively (**Figure 5f** and Figure S5c). Apart from high ORR performance, the NC-900 was made subject for methanol poisoning crossover effect. As can be seen in **Figure 5g**, the excellent resistance toward methanol was corroborated by mirror image of CV curves obtained with and without methanol injecting in the electrolyte solution during CV experiment. The catalyst also possesses a remarkable stability in alkaline solution. After a continuous chronoamperometric operation of 10 h, the NC-900 catalyst exhibited almost no attenuation in current density, while the commercial catalyst Pt/C displayed a decreased current of about 20% (**Figure 5h**). Based on the physical and electrochemical characterizations, the enhanced catalytic performance of the catalyst NC-900, overall can be concluded due to the unique morphology, abundance of mesoporous structure, and high content of nitrogen doping, promoting high mass and electron transport for ORR catalysis. The hierarchical coral-like nitrogen-doped carbon developed herein from the hybrid of polyaniline-silicon nitride presents appreciable ORR electrocatalysis as an alternative to Pt-based electrocatalysts.

4 | CONCLUSIONS

In conclusion, a coral-like nitrogen-doped carbon catalyst for ORR was successfully synthesized via self-assembly oxidative polymerization of aniline monomers on silicon nitride (Si_3N_4) nanospheres, followed by carbonization. The catalyst NC-900 showed outstanding oxygen reduction reaction activity by achieving an attractive onset potential of 0.90 V versus RHE and half-wave potential of 0.82 V versus RHE compared to the commercial Pt/C (η = 0.99 V vs. RHE and $E_{1/2}$ = 0.87 V vs. RHE) and many advanced metal-free carbon electrocatalyst recently reported in the literature. The catalyst NC-900 also revealed greater resistance toward methanol crossover and high stability than benchmark Pt/C catalyst in alkaline medium. This work provides a unique strategy to design electrocatalyst not only for ORR but can also be useful for other electrochemical energy conversion reactions.

ACKNOWLEDGMENTS

This study was financed in part by the Coordenação de Aperfeiçoamento de Pessoal de Nível Superior-Brasil (CAPES)-Finance Code 001. The author AMBH also would like to thank CWRU/Capes-Brazil program, Graduate program in Materials Science and Engineering of Federal University of São Carlos (PPG-CEM), Materials Engineering Department of Federal University of São Carlos and Macromolecular Science and Engineering Department of CWRU. MK would like to thank the São Paulo Research Foundation (FAPESP) for financial support under Grant No. 2017/00433-5.

DATA AVAILABILITY STATEMENT

The data used to support the findings of this research work are included within the article and Supporting Information, and more data may be available from the corresponding author on reasonable request.

CONFLICT OF INTEREST

The authors declare no conflict of interest.

ORCID

Ana Maria Borges Honorato https://orcid.org/0000-0002-4587-2668
Mohd. Khalid https://orcid.org/0000-0002-0305-531X
Luiz Antonio Pessan https://orcid.org/0000-0001-8363-9122

REFERENCES

1. J.L. Liu, D.D. Zhu, C.X. Guo, A. Vasileff, S.Z. Qiao, *Adv. Energy Mater.* **2017**, *7*, 1700518.
2. S. Li, C. Cheng, X.J. Zhao, J. Schmidt, A. Thomas, *Angew. Chem. Int. Ed.* **2018**, *57*, 1856.
3. Z.X. Pei, H.F. Li, Y. Huang, Q. Xue, Y. Huang, M.S. Zhu, Z.F. Wang, C.Y. Zhi, *Energy Environ. Sci.* **2017**, *10*, 742.
4. L. Yang, X.F. Zeng, W.C. Wang, D.P. Cao, *Adv. Funct. Mater.* **2018**, *28*, 1704537.
5. J.N. Chen, X.L. Yuan, F.L. Lyu, Q.X. Zhong, H.C. Hu, Q. Pan, Q. Zhang, *J. Mater. Chem. A*, **2019**, *7*, 1281.
6. L.L. Chen, Y.L. Zhang, X.J. Liu, L. Long, S.Y. Wang, W.X. Yang, J. B. Jia, *Chem. Commun.* **2019**, *55*, 5651.
7. L.N. Chong, J.G. Wen, J. Kubal, F.G. Sen, J.X. Zou, J. Greeley, M. Chan, H. Barkholtz, W. J. Ding, D.J. Liu, *Science* **2018**, *362*, 1276.

8. A.A. Gewirth, J.A. Varnell, A.M. Diascro, *Chem. Rev.* **2018**, *118*, 2313.
9. Y. Zheng, Y. Jiao, Y.H. Zhu, Q.R. Cai, A. Vasileff, L.H. Li, Y. Han, Y. Chen, S.Z. Qiao, *J. Am. Chem. Soc.* **2017**, *139*, 3336.
10. Z. Guan, X.J. Zhang, W.X. Chen, J.J. Pei, D. Liu, Y.R. Xue, W. Zhu, Z.B. Zhuang, *Chem. Commun.* **2018**, *54*, 12073.
11. R. Paul, F. Du, L. Dai, W. Yong, Z.L. Wang, F. Wei, A. Roy, *Adv. Mater.* **2019**, *31*, 1805598.
12. K. Gong, F. Du, Z. Xia, M. Durstock, L. Dai, *Science* **2009**, *323*, 760.
13. X. Liu, L. Dai, *Nat. Rev. Mater.* **2016**, *1*, 16064.
14. J. Zhang, Z. Xia, L. Dai, *Sci. Adv.* **2015**, *1*, e1500564.
15. A.M.B. Honorato, Mohd. Khalid, Q. Dai, L.A. Pessan, *Synth. Met.* **2020**, *264*, 116383.
16. Z. Qiu, N. Huang, J. Zhang, S. Zhou, P. Wang, *Int. J. Hydr. Ener.* **2019**, *44*, 32184.
17. J. Zhang, M. Lv, D. Liu, L. Du, Z. Liang, *Int. J. Hydr. Ener.* **2018**, *43*, 4311.
18. M. Kim, S. Cho, J. Song, S. Son, J. Jang, *ACS Appl. Mater. Interfaces*, **2012**, *4*, 4603.
19. S.-H. Lee, D.-H. Lee, K. Lee, C.-W. Lee, *Adv. Funct. Mater.* **2005**, *15*: 1495.
20. Z. Zhang, T. Zhao, B. Bai, L. Zeng, L. Wei, *Electrochim. Acta* **2017**, *248*, 194.
21. A.C. Ferrari, D.M. Basko, *Nat. Nanotech.* **2013**, *8*, 235.
22. S. Maldonado, K.J. Stevenson, *J. Phys. Chem. B* **2005**, *109*, 4707.
23. Y. Jiang, X. Wang, Y. Bao, W. Chen, L. Niu, *Nanoscale* **2014**, *6*, 15066.
24. L. Lai, J.R. Potts, D. Zhan, L. Wang, C.K. Poh, C. Tang, H. Gong, Z. Shen, J. Lin, R.S. Ruoff, *Ener. Environ. Sci.* **2012**, *5*, 7936.
25. J. Zhang, L. Dai, *ACS Catal.* **2015**, *5*, 21.
26. Z.H. Sheng, L. Shao, J.J. Chen, W.J. Bao, F.B. Wang, X.H. Xia, *ACS Nano*, **2011**, *5*, 4350.
27. R. Liu, D. Wu, X. Feng, K. Müllen, *Angew. Chem. Int. Ed.* **2010**, *49*, 2565.
28. C.G. Hu, Y. Xiao, Y. Zhao, N. Chen, Z.P. Zhang, M.H. Cao, L.T. Qu, *Nanoscale* **2013**, *5*, 2726.
29. L.T. Qu, Y. Liu, J.-B. Baek, L.M. Dai, *ACS Nano*. **2010**, *4*, 1321.
30. J. Liang, Y. Jiao, M. Jaroniec, S.Z. Qiao, *Angew. Chem. Int. Ed.* **2012**, *51*, 11496.
31. H. Yu, X. Ning, J. Ming, Q. Wang, H. Wang, Y. Cao, F. Peng, Y. Yang. *Chem. Sci.* **2019**, *10*, 1589.
32. C. Huang, C. Li, G. Shi, *Ener. Environ. Sci.* **2012**, *5*, 8848.
33. J.P. Paraknowitsch, A. Thomas, *Ener. Environ. Sci.* **2013**, *6*, 2839.
34. S. Liu, Z. Wang, S. Zhou, F. Yu, M. Yu, C.Y. Chiang, W. Zhou, J. Zhao, J. Qiu, *Adv. Mater.* **2017**, *29*, 1700874.
35. J.J. Zhang, G. Yin, W. Xing. *Rotating electrodes methods and oxygen reduction electrocatalysts*. Brazil: Elsevier. **2014**.

SUPPORTING INFORMATION

Additional supporting information may be found online in the Supporting Information section at the end of the article.

How to cite this article: A. M. Borges Honorato, M. Khalid, L. A. Pessan, *Electrochem. Sci. Adv.* **2021**, *1,* e2000010. https://doi.org/10.1002/elsa.202000010